Classical Theory of Atom Scattering from Corrugated Surfaces

W. W. Hayes

Physical Sciences Department

Greenville Technical College

Greenville, SC, 29606, USA[*]

J. R. Manson

Department of Physics and Astronomy, Clemson University

Clemson, South Carolina 29634, U.S.A.[†]

(Dated: March 29, 2013)

Abstract

A theory based in the semiclassical eikonal approximation is developed to describe energy transfer in the collision of an atomic projectile with a surface which is either ordered or disordered. This theory is extended from the quantum mechanical regime to the classical regime of complete quantum decoherence via the Bohr correspondence principle of large numbers of excited quanta. In the quantum mechanical regime the theory reproduces the well-known eikonal approximation for elastic collisions, provides a simple and useful expression for single phonon inelastic scattering, and leads to further expressions for multiple phonon transfers. In the classical limit the theory produces an expression that includes the effects of surface corrugation in addition to the excitations of large numbers of phonons. This new theory shows that a simple measurement of the most probable intensity of energy-resolved scattering spectra taken as a function of surface temperature, with all other experimentally controllable parameters held fixed, can be used to extract the surface corrugation amplitude. Comparisons with data for Ar scattering from the molten metals Ga and In shows good agreement with the measured energy resolved spectra, the in-plane angular distributions, the out-of-plane angular distributions and produces values for the corrugation amplitudes that range from 10 to 30% of the average interparticle spacing.

I. INTRODUCTION

Essential for detailed understanding of gas-surface interactions is knowledge of the interaction energy landscape. The energy landscape can be viewed as the height of the classical turning point of the interaction potential energy evaluated at each point $\mathbf{R}$ lateral to the surface plane. Knowledge of the landscape is essential for predicting chemical reactions at surfaces as well as heterogeneous catalysis and is necessary for calculating the results of state-to-state scattering experiments. If the surface is regarded as a hard repulsive barrier defined by the classical turning point then the energy landscape can be uniquely characterized by a corrugation function $\xi(\mathbf{R})$ which gives the position of the corrugated barrier relative to a reference plane.

The usual way of obtaining the corrugation function of the surface energy landscape is through comparisons with calculations of state-to-state measurements using well-defined molecular beams scattering experiments. The most extensive and accurate experiments have been carried out in the quantum mechanical regime using low energy helium atom projectiles and relatively low surface temperatures.[1–4] In the most precise of such experiments extremely accurate and extensive evaluations of the interaction potentials have been obtained.[5] However, many experiments have been carried out in the regime of large projectile masses, high incident energies and large surface temperatures where large numbers of quanta are transferred during the interaction, the scattering becomes decoherent and all detailed quantum features disappear. Under such conditions the scattering can be treated with classical mechanics, but still a significant amount of information about the interaction potential can be obtained by comparison of calculations with experimental measurements.[6–13]

In this classical regime all sharp and detailed quantum features, such as diffraction peaks, single phonon peaks and diffuse elastic peaks are suppressed and disappear, and the energy-resolved spectra consist of rather broad structures that further broaden with increasing surface temperature. In many cases the energy-resolved scattering spectra consist of a single broad peak, such as the case of amorphous surfaces,[14,15] while for ordered surfaces multiple broad peaks may appear as a result of rainbow features.[7,9–12]

The purpose of this paper is to develop a semiclassical theory of atom-surface scattering, based on the eikonal approximation,[16,17] that can include inelastic transfers with the phonons. This theory provides a simple, but useful expression for describing the quantum

mechanical limit of single phonon transfers in atom-surface collisions. However, of importance for the purposes of this paper it also provides a way of obtaining useful expressions in the classical multiphonon limit of large numbers of quanta transferred. This transition to the classical limit is an example of the application of the Bohr correspondence principle of large quantum numbers.

The result of interest presented here is a classical theory of atom-surface scattering in the impulsive limit, e.g., the limit of short collision times, that can treat rough or periodic surfaces and is capable of treating rainbow patterns that can be exhibited by periodic surfaces. An interesting result that was predicted some time ago,[18] but only recently verified in comparisons of calculations with experimental measurents,[19] is that a relatively simple temperature-dependent measurement of the scattered spectrum can be used to determine the amplitude of the surface corrugation. Namely, for both amorphous or periodic surfaces, the dependence on temperature of the most probable intensity of the typically observed energy-resolved scattered spectra gives directly a measure of the average corrugation amplitude of the energy landscape.

That such a simple measurement should be useful for providing information on the surface corrugation function is evident from comparing two different, but well-known theoretical expressions for the transition rate $w(\mathbf{p}_f, \mathbf{p}_i)$ from which one can obtain the differential cross section for scattering in the classical limit of an atomic projectile in the initial state of momentum $\mathbf{p}_i$ to a final state of momentum $\mathbf{p}_f$. These equations describe the extremes of a surface that is highly corrugated and thermally vibrating, or one that is regarded as being flat except for small time-dependent thermal corrugations.

The highly corrugated system is represented by an atomic projectile of mass m colliding with discrete scattering centers of mass M_S that are initially moving with an equilibrium distribution of velocities at temperature T_S[20,21]

$$w(\mathbf{p}_f, \mathbf{p}_i) \;\propto\; \sqrt{\frac{1}{4\pi k_B T_S \Delta E_0}}\; |\tau_{fi}|^2 \;\exp\left\{ -\frac{(E_f - E_i + \Delta E_0)^2}{4 k_B T_S \Delta E_0} \right\} \;, \tag{1}$$

where $\Delta E_0 = (\mathbf{p}_f - \mathbf{p}_i)^2/2M_S$ is the binary collision recoil energy, k_B is the Boltzmann constant and the transition matrix element τ_{fi} is determined by the interaction potential.

Regarded as a function of final energy E_f the transition rate of Eq. (1) typically appears as a structure with a single peak whose shape is primarily determined by the Gaussian-like exponential function. The temperature dependence of the width is governed largely

by the factor of T_S in the argument of this exponential, which gives an approximate $\sqrt{T_S}$ dependence on the full width at half maximum (FWHM) which is behavior typical for classical scattering. The most probable intensity occurs very near the final energy for which the argument of the exponential vanishes, implying that the temperature dependence of the most probable intensity (at the maximum peak positon) is governed by the prefactor and consequently varies as $1/\sqrt{T_S}$.

The transition rate for an uncorrugated surface, i.e., a surface with no static corrugation, but which has small time-dependent thermal displacements caused by the underlying motions of the bulk atoms is[22–25]

$$w(\mathbf{p}_f, \mathbf{p}_i) \;\propto\; \frac{1}{(4\pi k_B T_S \Delta E_0)^{3/2}}\; |\tau_{fi}|^2 \;\exp\left\{ -\frac{(E_f - E_i + \Delta E_0)^2 + 2v_R^2 \mathbf{P}^2}{4 k_B T_S \Delta E_0} \right\}\,, \qquad (2)$$

where $\mathbf{P}$ is the component of the momentum transfer vector $\mathbf{p} = \mathbf{p}_f - \mathbf{p}_i$ parallel to the surface and v_R is a parameter having dimensions of speed, but which is completely determined by the phonon distribution. It is a weighted average over the distribution of phonon velocities at the surface.[23]

Eq. (2) differs from Eq. (1) by the additional Gaussian-like factor in $\mathbf{P}^2$ and the prefactor, or envelope function, is raised to the 3/2 power as opposed to the square root. Under most experimental conditions Eq. (2), like Eq. (1), is also a single-peaked function of the final energy E_f with the most probable intensity occurring near the final energy E_f at which the total combined argument of the exponential is a minimum. In this case the temperature dependence of the most probable intensity is approximately that implied by the prefactor, which has the functional dependence given by $1/T_S^{3/2}$.

It should be noted that the form factor $|\tau_{fi}|^2$ appearing in Eq. (2) does not appear in the original derivation of the scattering cross section of Brako and Newns.[23] This is because Brako and Newns considered in their derivation only the inelastic part of the interaction potential, and in fact, only the part of the inelastic interaction potential that is linear in the phonon displacements. The need for the form factor $|\tau_{fi}|^2$ becomes apparent when one includes the effects of the elastic part of the interaction potential, which is the part of the potential that guides the projectile towards the surface before collision and away from the surface after the collision. To make this point explicit, the total interaction potential between an incoming atomic projectile and a vibrating surface $V(\mathbf{r}, \mathbf{u})$ is usually expanded

as a power series in the phonon displacements signified by $\mathbf{u}$

$$V(\mathbf{r},\mathbf{u}) \;=\; V(\mathbf{r},\mathbf{u})|_{\mathbf{u}=0} \;+\; \nabla_{\mathbf{u}}\, V(\mathbf{r},\mathbf{u})|_{\mathbf{u}=0}\cdot\mathbf{u} + \ldots \;, \tag{3}$$

and often the assumption is made that $V(\mathbf{r},\mathbf{u}) = V(\mathbf{r}+\mathbf{u})$ in which case the gradient with respect to the phonon displacements $\mathbf{u}$ can be replaced by the gradient with respect to the position variable $\mathbf{r}$. The leading term on the right hand side of Eq. (3) is called the elastic potential since it does not contribute to energy exchange with the surface. The second term on the right is the term linear in the phonon displacements and it is through using this part of the potential in the impulse approximation that leads to the original Brako-Newns formula.[23] Higher order terms in the expansion of Eq. (3) are usually neglected, and in fact have been shown to contribute negligibly to the energy transfer for scattering of rare gases from surfaces.[28] Although Brako and Newns ignored the elastic part of the potential in their treatment, it is inclusion of the elastic potential that gives rise to the form factor $|\tau_{fi}|^2$. The need for such a form factor can be most simply demonstrated by obtaining Eqs. (1)and (2) by using the kinematical approximation.[22] A more general treatment based on the full potential of Eq. (3) identifies τ_{fi} as the transition matrix of the elastic potential extended off the energy shell in order to account for energy transfer to the surface via excitation of phonon quanta.[25]

The sharply contrasting behaviors of the most probable intensity temperature dependence, i.e., those of Eq. (1) and (2), have been observed in scattering experiments. The $1/T_S^{1/2}$ behavior for scattering from a highly corrugated discrete particle target surface was clearly observed for the scattering of low-energy alkali atom ions from a Cu(001) surface.[26] Corresponding to the case of an uncorrugated surface, a temperature dependence behaving very nearly as $1/T_S^{3/2}$ has been verified using the two similar mass projectiles ^{4}He atoms and D_2 molecules scattering under classical conditions at hyperthermal energies from a clean Cu(001) surface.[27]

The simple and straightforward comparison of the most probable intensities provided by Eqs. (1) and (2) shows that there is a distinct difference in temperature dependence, with the intensity of a strongly corrugated surface behaving as $1/T_S^{1/2}$ while that of an uncorrugated surface having a significantly stronger dependence going approximately as $1/T_S^{3/2}$. The logical conclusion from this observation is that a moderately corrugated surface should exhibit a temperature dependence intermediate between these two extreme behaviors.[18,29,30] Thus, a measurement of the temperature dependence of the most probable intensity of

the energy-resolved scattering spectra allows one to extract the strength of the corrugation when experimental measurements are compared with appropriate theory. This is a major conclusion drawn from the theory and comparisons with experimental data presented in this paper.

II. THEORY

Although the ultimate objective is to obtain a classical theory of atom-surface scattering that can include the surface corrugation, the simplest approach actually is to begin from a quantum mechanical treatment and then go to the classical limit of large quantum numbers. With this approach in mind an appropriate starting point is the generalized Fermi Golden Rule

$$w(\mathbf{p}_f, \mathbf{p}_i) \;=\; \frac{2\pi}{\hbar} \left\langle \sum_{\{n_f\}} |T_{fi}|^2 \delta(\mathcal{E}_f - \mathcal{E}_i) \right\rangle \;, \tag{4}$$

where T_{fi} is the transition matrix element taken with respect to final and initial states of the system of projectile plus target surface, $\mathcal{E}_i$ and $\mathcal{E}_f$ are the initial and final energies of the entire system and $\hbar$ is Planck's constant. The angular brackets signify an average over all initial states of the surface and the $\sum_{\{n_f\}}$ indicates a sum over all final states of the target.

The transition matrix T_{fi} will be developed in the semiclassical limit using the eikonal approximation as developed for a hard repulsive potential with a corrugation function $\xi(\mathbf{R})$.[16,17] This was originally formulated for the purely elastic scattering problem of a quantum mechanical projectile colliding with a hard corrugated wall. In the asymptotic region far in front of the surface the elastic wave function has the form

$$\psi_i(\mathbf{r}) \;=\; e^{i\mathbf{p}_i\cdot\mathbf{r}/\hbar} \;-\; \sum_{\mathbf{P}} \; A(\mathbf{P}) \; e^{i(\mathbf{P}_i+\mathbf{P})\cdot\mathbf{R}/\hbar} \; e^{ip_{fz}z/\hbar} \;, \tag{5}$$

The eikonal approximation consists of two assumptions. First, the Rayleigh ansatz which assumes that the asymptotic wave function of Eq. (5) can be extended through the selvege region up to the position of the hard wall at $z = \xi(\mathbf{R})$, and second, that the final momentum perpendicular to the surface p_{fz} is weakly dependent on parallel momentum transfer $\mathbf{P}$. For the elastic transition matrix associated with the elastic part of the potential (i.e., the first term on the right side of Eq. (3)) the eikonal approximation leads to

$$T_{fi} \;=\; ie^{i\delta_f} \; \frac{\hbar p_{fz}}{mL} \; \frac{1}{L^2} \; \int \; d\mathbf{R} \; e^{-i\mathbf{P}\cdot\mathbf{R}/\hbar} \; e^{-i\Delta p_z \xi(\mathbf{R})/\hbar} \;, \tag{6}$$

where $\Delta p_z = p_{iz} + p_{fz}$ is the momentum transfer in the direction normal to the surface, L is a quantization length, and δ_f is a phase that is unimportant in calculating the transition rate of Eq. (4).

In order to add the effect of thermal vibrations on the transition rate the repulsive surface is regarded as having a time and position dependent vibrational displacement denoted by $\mathbf{u}(\mathbf{R},\mathbf{t}) = \{\mathbf{U}(\mathbf{R},t), u_z(\mathbf{R},t)\}$. Then in Eq. (6) we have $\mathbf{R} \longrightarrow \mathbf{R} - \mathbf{U}(\mathbf{R},t)$ and $\xi(\mathbf{R}) \longrightarrow \xi(\mathbf{R}) - u_z(\mathbf{R},t)$ leading to a transition matrix taking the form

$$T_{fi} \;=\; ie^{i\delta_f}\;\frac{\hbar p_{fz}}{mL}\;\frac{1}{L^2}\;\int\; d\mathbf{R}\;\; e^{-i\mathbf{P}\cdot\mathbf{R}/\hbar}\quad e^{-i\Delta p_z \xi(\mathbf{R})/\hbar}\;\; e^{i\mathbf{p}\cdot\mathbf{u}(\mathbf{R},t)/\hbar}\;. \tag{7}$$

The transition matrix of Eq. (7) is a special example of the kinematic approximation that has been successfully applied to X-ray, neutron and electron scattering. In the kinematic approximation the transition operator for each lattice position in the crystal is multiplied by the phonon displacement operator $\exp\{i\mathbf{p}\cdot\mathbf{u}/\hbar\}$.

The sum and average over target states in Eq. (4) can now be carried out in a straightforward manner using the Glauber-Van Hove transformation:[31,32]

$$w(\mathbf{p}_f,\mathbf{p}_i) \;=\; \frac{1}{\hbar^2}\;\left(\frac{\hbar^2 k_{fz}}{mL}\right)^2\;\;\int_{-\infty}^{+\infty} dt\; e^{i(E_i-E_f)t/\hbar} \tag{8}$$
$$\times\;\;\frac{1}{L^4}\;\int\; d\mathbf{R}\;\int\; d\mathbf{R}'\; e^{-i\mathbf{P}\cdot(\mathbf{R}-\mathbf{R}')/\hbar}\; e^{-i\Delta p_z[\xi(\mathbf{R})-\xi(\mathbf{R}')/\hbar]}\left\langle e^{i\mathbf{p}\cdot\mathbf{u}(\mathbf{R},t)/\hbar} e^{-i\mathbf{p}\cdot\mathbf{u}(\mathbf{R}',0)/\hbar}\right\rangle\;.$$

Assuming displacements in the harmonic approximation leads to expressions involving the displacement-displacement correlation function

$$2\mathcal{W}(\mathbf{p};\mathbf{R},\mathbf{R}',t) \;=\; \left\langle\; \mathbf{p}\cdot\mathbf{u}(\mathbf{R},t)\;\mathbf{p}\cdot\mathbf{u}(\mathbf{R}',0)/\hbar^2\;\right\rangle\;. \tag{9}$$

and the transition rate takes the form

$$w(\mathbf{p}_f,\mathbf{k}_i) \;=\; \frac{1}{\hbar^2}\;\left(\frac{\hbar^2 k_{fz}}{mL}\right)^2\;\;\int_{-\infty}^{+\infty} dt\; e^{i(E_i-E_f)t/\hbar} \tag{10}$$
$$\times\;\;\frac{1}{L^4}\;\int\; d\mathbf{R}\;\int\; d\mathbf{R}'\; e^{-i\mathbf{P}\cdot(\mathbf{R}-\mathbf{R}')/\hbar}\; e^{-i\Delta p_z[\xi(\mathbf{R})-\xi(\mathbf{R}')/\hbar]}\; e^{-2W(\Delta\mathbf{p})}\; e^{2\mathcal{W}(\mathbf{p};\mathbf{R},\mathbf{R}',t)}\;.$$

where the argument of the Debye-Waller factor $\exp\{-2W\}$ is given by

$$2W(\mathbf{p}) \;=\; \left\langle(\mathbf{p}\cdot\mathbf{u})^2/\hbar^2\right\rangle\;. \tag{11}$$

Equation (10) is a fully quantum mechanical scattering transition rate for a hard repulsive potential within the eikonal approximation.[17] The elastic and single phonon limits are obtained upon expanding the exponentiated correlation function in powers of $2\mathcal{W}(\mathbf{p};\mathbf{R},\mathbf{R}',t)$,

and for completeness these are developed in the Appendix A. Of interest here, however, is the the classical scattering limit which can be obtained from Eq. (10) by applying the Bohr correspondence principle of large numbers of quanta transferred in the collision.

The classical limit is achieved when large numbers of phonon quanta are created and destroyed in which case the scattering process becomes completely incoherent. The value of the argument $2W$ of the Debye-Waller factor is a measure of the number of phonons transferred in the collision and it becomes large in the classical limit of large energies or when the mean square displacement (effectively the temperature) becomes large.

When the Debye-Waller argument $2W$ becomes large the most important contributions to the correlation function $2\mathcal{W}$ of Eq. (9) come from the region of small t and small $\mathbf{R}-\mathbf{R}'$. In this case the correlation function can be evaluated as an expansion. The simplest approximation for evaluating the expansion is to assume a Debye model with bulk-like symmetry in which all cross terms vanish and this leads to

$$2\mathcal{W}(\mathbf{p};\mathbf{R},\mathbf{R}',t) \;\approx\; 2W(\mathbf{p}) - i\Delta E_0 t - \Delta E_0 k_B T_S t^2 - \frac{\Delta E_0 k_B T_S (\mathbf{R}-\mathbf{R}')^2}{2\hbar^2 v_R^2} \;+\; \ldots\,, \quad (12)$$

where the classical recoil energy is given as in Eq. (1) by $\Delta E_0 = \mathbf{p}^2/2M_S$, and the velocity parameter v_R is a weighted average of phonon velocities parallel to the surface.[23] For several simple models of the surface phonon density v_R can be evaluated and these models produce values that are of order of the bulk acoustic phonon velocities or the Rayleigh wave velocity.

Insertion of the classical limit expansion of Eq. (12) into the transition rate of Eq. (10) gives rise to two big simplifications. First, the time and double-spatial integrals separate into two simpler product functions. Second, and this is the hallmark of the classical transition, the leading term in the expansion of Eq. (12) exactly cancels the Debye-Waller factor. Thus, in spite of the fact that the Debye-Waller factor becomes vanishingly small and suppresses all quantum features, in the classical limit it is canceled out leaving behind a function exhibiting the broader features characteristic of classical scattering. The time integral can be carried out using the method of steepest descents and the result is

$$w(\mathbf{p}_f,\mathbf{p}_i) \;=\; \left(\frac{p_{fz}}{mL}\right)^2 \frac{2\pi\hbar}{\sqrt{4\pi\Delta E_0 k_B T_S}} \;\exp\left\{-\frac{(E_f - E_i + \Delta E_0)^2}{4\Delta E_0 k_B T_S}\right\} \quad (13)$$

$$\times\; \frac{1}{L^4}\int d\mathbf{R}\int d\mathbf{R}'\; e^{-i\mathbf{P}\cdot(\mathbf{R}-\mathbf{R}')/\hbar}\; e^{-i\Delta p_z[\xi(\mathbf{R})-\xi(\mathbf{R}')]/\hbar}\; \exp\left\{-\frac{\Delta E_0 k_B T_S (\mathbf{R}-\mathbf{R}')^2}{2\hbar^2 v_R^2}\right\}.$$

In Eq. (13) the leading terms appearing before the spatial integrals are identical with the transition rate of Eq. (1), showing that if the displacement correlations arising from the

flat surface are completely ignored the transition rate becomes the form of Eq. (1) for a discrete surface. Alternatively, if the corrugation function $\xi(\mathbf{R})$ is set equal to a constant value corresponding to a smooth plane, then the spatial integrals can also be carried out using methods of steepest descents and the result is that of Eq. (2). The overall product factors of p_{fz} are identified with the transition matrix τ_{fi} appearing in Eq. (2) for the case of a hard repulsive potential. Eq. (13) is the central result used in this paper.

III. COMPARISON WITH EXPERIMENTS

The first angular distributions measured for the scattering of atoms from surfaces were carried out by Stern and coworkers and these used a thermal beam of low-energy He atoms or H_2 molecules scattered from alkali halide surfaces.[33,34] A resurgence of interest in this field resulted from the development of the supersonic molecular jet which provided energetically well-defined beams of molecular and atomic projectiles.[35,36] The modern history of energy-resolved measurements in the classical regime which is usually defined by large mass projectiles, high incident energies and large surface temperatures started with the seminal experiments of Hurst *et al.* that reported the results of a supersonic beam of Xe atoms reflected from a Pt(111) surface.[37] However, in spite of a history of a large number of energy-resolved scattering experiments carried out since, many of which even reported varying aspects of temperature dependent measurements, essentially none reported the type of experiments that we are suggesting here which are energy-resolved spectra with relative intensity measurements over a range of different temperatures with all other controllable parameters remaining fixed. In fact, to our knowledge there is only one series of experiments reporting reliable relative intensity measurements as a function of surface temperature and this is the work of Nathanson *et al.* for the scattering of Ar from the molten metals indium and gallium.[14,15] This is the work that we analyze here using the theory of the above Sec. II.

Figure 1 shows the three energy resolved spectra taken for in-plane Ar scattering from molten Ga at three different temperatures of 313, 483 and 673 K. The incident energy is 95 kJ/mol (0.99 eV) and the incident angle is 55° and the final angle is at the specular position, i.e., $\theta_i = \theta_f = 55°$. The experimental data are shown as open circles and consist of a single broad peak, characteristic of scattering in the classical regime, and a shoulder at low energies. The most probable energy shows a typical energy loss of about one-third of

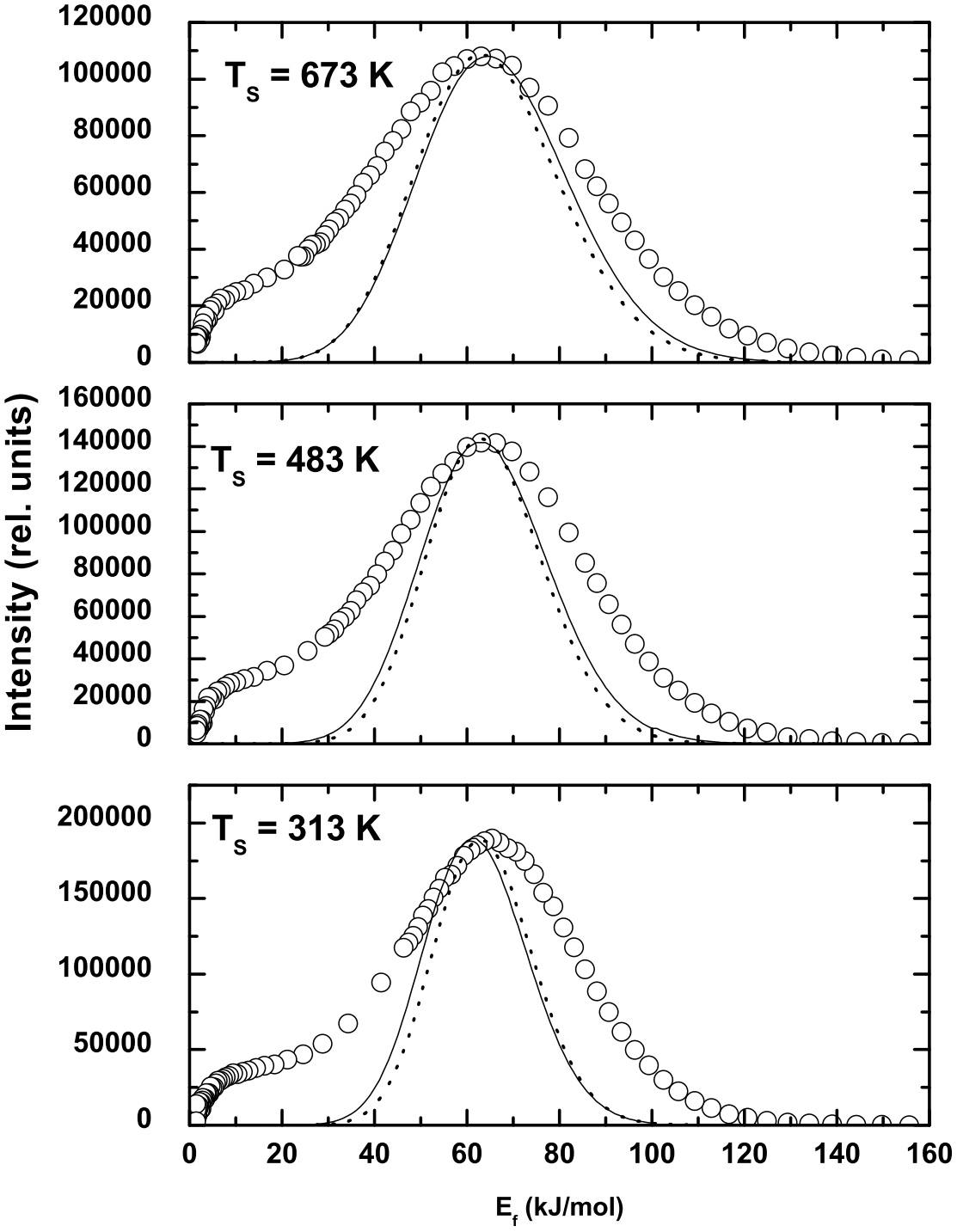

FIG. 1: Energy resolved spectra for Ar scattering from molten Ga at three different temperatures $T_S = 313$, 483 and 673 K as marked. The incident energy is 95 kJ/mol and the incident and final angles are $\theta_i = \theta_f = 55°$. Data are from Nathanson *et al.*[14].

the incident energy. It is evident that as the Ga temperature is increased the full width at half maximum (FWHM) of the peak broadens and the most probable intensity decreases. This behavior is consistent with the principle of unitarity, the assumption that the total flux of particles scattered from the surface equals the flux of incident particles, i.e., as the temperature increases the particles are scattered over a broader energy range and to conserve the number of particles the maximum intensity decreases concomitantly. Two calculations are shown in each panel of Fig. 1, the solid curve is carried out using the transition rate for a corrugated surface of Eq. (13) with the a characteristic corrugation of the liquid surface as discussed in the following paragraph and the dotted curve is for a flat surface with no static corrugation. Both of these calculations are for a single collision of the Ar projectile with the Ga surface and they do not exhibit the shoulder feature that is apparent in the data at very low energies (i.e., at large energy loss). These shoulder features have been demonstrated to be due to double scattering in which each of the two collisions occurs with a large scattering angle, and are discussed further below in connection with Fig. 5.

In the classical scattering regime all quantum mechanical interference arising from waves reflected from different parts of the surface is suppressed. Thus the surface integrals in the transition rate of Eq. (13) can be limited to a single characteristic scattering center of the surface. For the interaction of Ar with the molten metal a sinusoidal function representing the boss presented by a surface metal atom is chosen for the corrugation function:

$$\xi(\mathbf{R}) \;=\; ha\cos\left(\frac{2\pi R}{a}\right)\;, \tag{14}$$

where a is taken to be the average interatomic spacing in the bulk liquid, $\mathbf{R}$ is the two-dimensional displacement parallel to the surface and R is its magnitude which ranges from zero to $a/2$. This gives a corrugation profile for a typical surface atom with a trough-to-crest height of $2ha$, or a root mean square amplitude of $ha/\sqrt{2}$.

The solid curves shown in Fig. 1 were calculated with the transition rate of Eq. (13) using the corrugation function of Eq. (14) and a corrugation height $h = 0.13$ which for the Ga interatomic distance of $a = 2.78$ Å gives a corrugation amplitude $ha = 0.36$ Å. The two other parameters necessary for the calculations are v_R and the effective surface mass M_S and these were determined from an earlier analysis of this same data using the smooth surface model of Eq. (2) to be $v_R = 600$ m/s and $M_S = 1.65$ times the mass of a single Ga atom, or 115 amu.[38] In the three panels of Fig. 1 the solid curve calculations are normalized

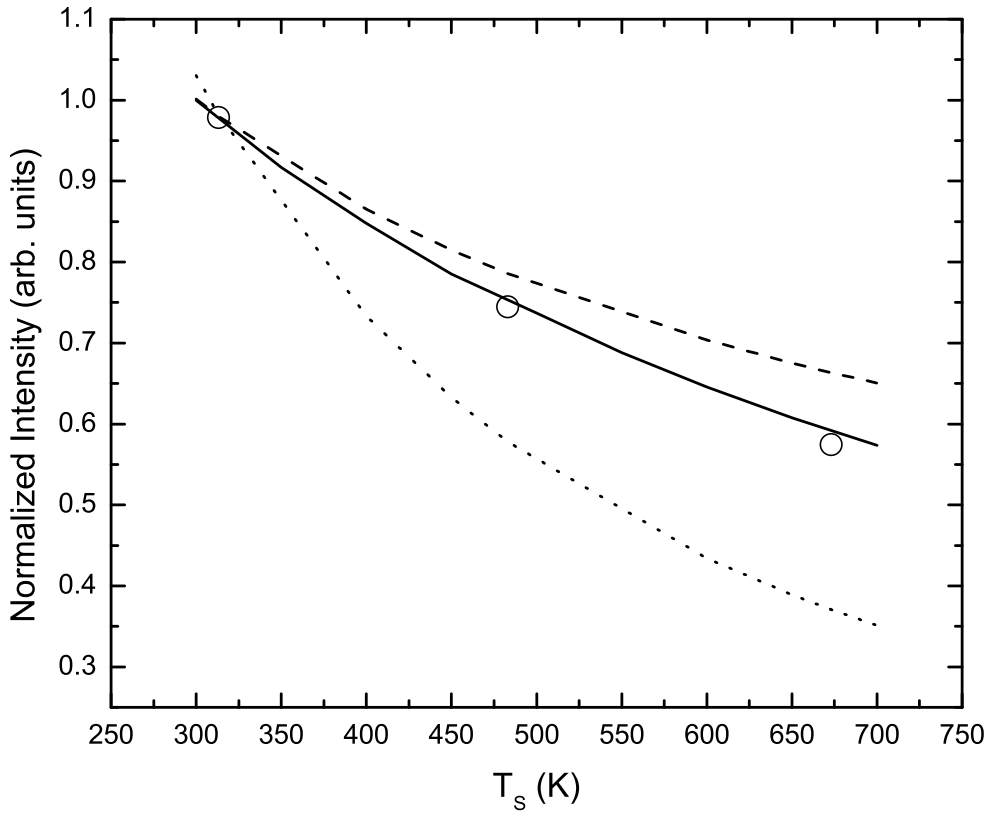

FIG. 2: Temperature dependence of the most probable intensity for Ar scattering from molten Ga at incident energy $E_i = 95$ kJ/mol, and incident and final angles $\theta_i = \theta_f = 55°$. The experimental data are shown as open circles and the solid curve is the calculation for a corrugated surface. The dashed curve is the result of the discrete surface theory of Eq. (1) and the dotted curve is for the smooth uncorrugated surface model of Eq. (2).

to the experimental data only for the lowest panel at the temperature 313 K and the other two panels show actual relative intensities. The dotted curve calculations, done with the uncorrugated statically flat surface calculation, are normalized to the data in each individual panel. This need for a difference in normalization is evident from the comparisons of the temperature dependence shown in Fig. 2, where it is seen that the temperature dependence of the uncorrugated theory is substantially stronger than that of the corrugated surface theory.

Figure 2 plots the most probable intensity of each of the spectra shown in Fig. 1 as a function of molten Ga temperature. The experimental values are represented as circles, the dashed curve is the $1/\sqrt{T_S}$ behavior of the highly-corrugated discrete surface model of Eq. (1), and the dotted curve is the nearly ${1/T_S}^{3/2}$ behavior of the statically uncorrugated smooth surface model of Eq. (2). The solid curve is the fit to the experimental data using the corrugated model theory of Eq. (13) with the corrugation function of Eq. (14) and the best fit corrugation height $h = 0.13$.

It is interesting to note that the temperature dependence plotted in Figure 2 exhibits a significant difference in behavior between the results of the corrugated surface and those of the uncorrugated surface. The corrugated surface exhibits a much weaker decrease in maximum intensity, in fact relatively close to that of the highly corrugated discrete surface, than the strong nearly ${1/T_S}^{3/2}$ decreasing behavior of the uncorrugated surface. This behavior contrasts sharply with the two calculations shown in each panel of Fig. 1 where the shapes (but not the relative intensities) of the two different curves are quite similar. This fact illustrates an important point that is to be drawn from the calculations presented here and that is that merely comparing normalized calculations to the presently available data, all of which is taken at or near specular conditions which corresponds to the neighborhood of the maximum scattered intensities, is not sufficient to detect differences in the corrugation of the interaction potential. Instead, it is in the temperature dependence of the scattered intensities that the surface corrugation more strongly manifests its presence.

The ability of a relatively simple temperature dependent measurement to reveal the corrugation parameter is the central problem addressed in this paper, but to make this result more convincing the corrugated theory must be capable of explaining all available scattering data for the system. That this is the case is exhibited in the following Figs. 3 and 4 which show two independent types of angular distributions that were measured for Ar scattering from molten Ga at the same incident angle and nearly the same energy as in Fig. 1.

The experimental points shown as open circles in Fig. 3 show a series of three in-plane angular distributions for Ar/Ga with an incident energy of 92 kJ/mol (0.95 meV) and temperatures of 308, 436 and 586 K as marked. For the fixed incident angle of 55° what is plotted is the total intensity collected as a function of final detector angle regardless of energy. Since these experiments were carried out with a stagnation-type detector the exper-

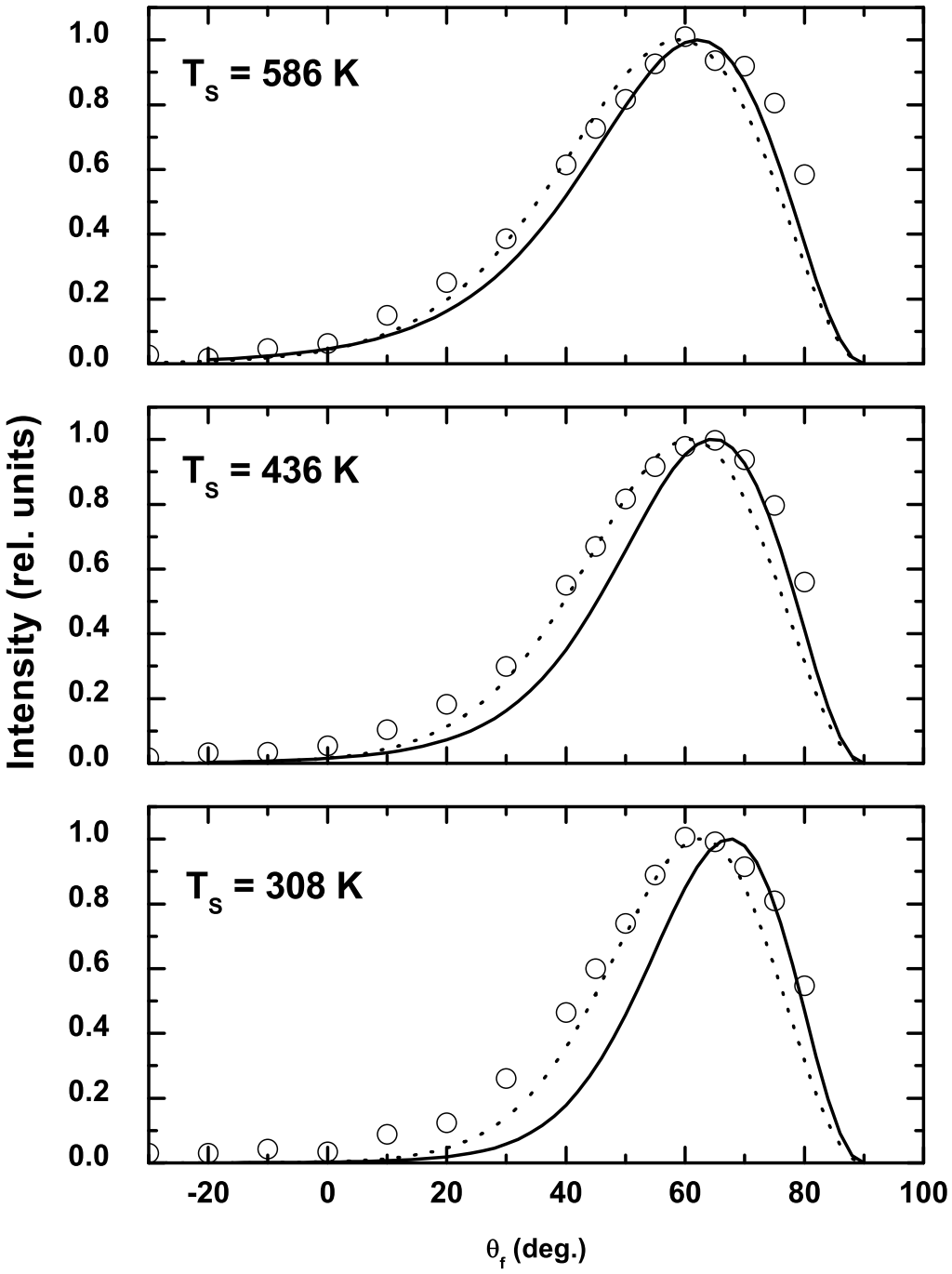

FIG. 3: In-plane angular distributions for Ar scattering from molten Ga with incident energy $E_i = 92$ kJ/mol and incident polar angle $\theta_i = 55°$. The liquid Ga temperatures are $T_S = 308,\ 436,$ and 586 K as marked. Open circles are the data[14], the solid curve is the present calculation for a corrugated surface, and the dotted curve is for an uncorrugated surface.

imental results at each angle can be compared with the integral over all final energies of the theoretical differential reflection coefficient, i.e., there is no detector correction that needs to be applied. The experimental results present a single broad peak with a supraspecular maximum intensity at a position approximately 10° greater than the specular angle of 55°. There is a sharp cut-off in intensity as the scattering angle increases towards the grazing angle of $\theta_f = 90°$, and there is a long subspecular tail extending well into the quadrant of the incident beam. Two calculations are shown as in Figs. 1 and 2, the solid curve is the calculation for the corrugated surface and the dotted curve is for the uncorrugated surface. Both of the theoretical curves have been normalized near the maximum in the data in each of the three panels because these angular distribution experiments did not produce good relative intensities for different liquid surface temperatures. It is evident that both sets of calculations agree reasonably with the experiment, and exhibit relatively insignificant differences. The most notable difference is that the corrugated surface calculation is slightly narrower in width than the uncorrugated calculation, a result caused by the fact that its energy-resolved intensities tend to be somewhat larger near the region of maximum in the angular distribution. However, consistent with what we have previously said there is relatively little that can be discerned about the difference in interaction potential by comparing the two different calculations to the angular distributions.

Three out-of-plane angular distributions are shown in Fig. 4, taken for the same temperatures and incident energy as Fig. 3. In these measurements the incident and polar angles are fixed at $\theta_i = \theta_f = 55°$ and the same detector as in Fig. 3 is moved at fixed height above the surface in the direction perpendicular to the scattering plane. The intensity is reported as a function of the angle α_f which is the angle whose tangent is the distance of the detector from the scattering plane divided by the vertical height of the detector above the surface. As in Fig. 3 the data are reported in arbitrary units so the calculations are normalized to the data at one point for each of the three temperatures. Both the uncorrugated and corrugated surface calculations give a reasonable explanation of the data, but as expected the corrugated calculation exhibits a somewhat broader out-of-plane angular distribution than that of the uncorrugated surface because two mechanisms rather than one, both phonon excitation and corrugation, are present in these calculations. However, once again the small difference between the two calculations and the fact that both compare well with the data illustrates the fact that, at least over the range of the present measurements, comparing

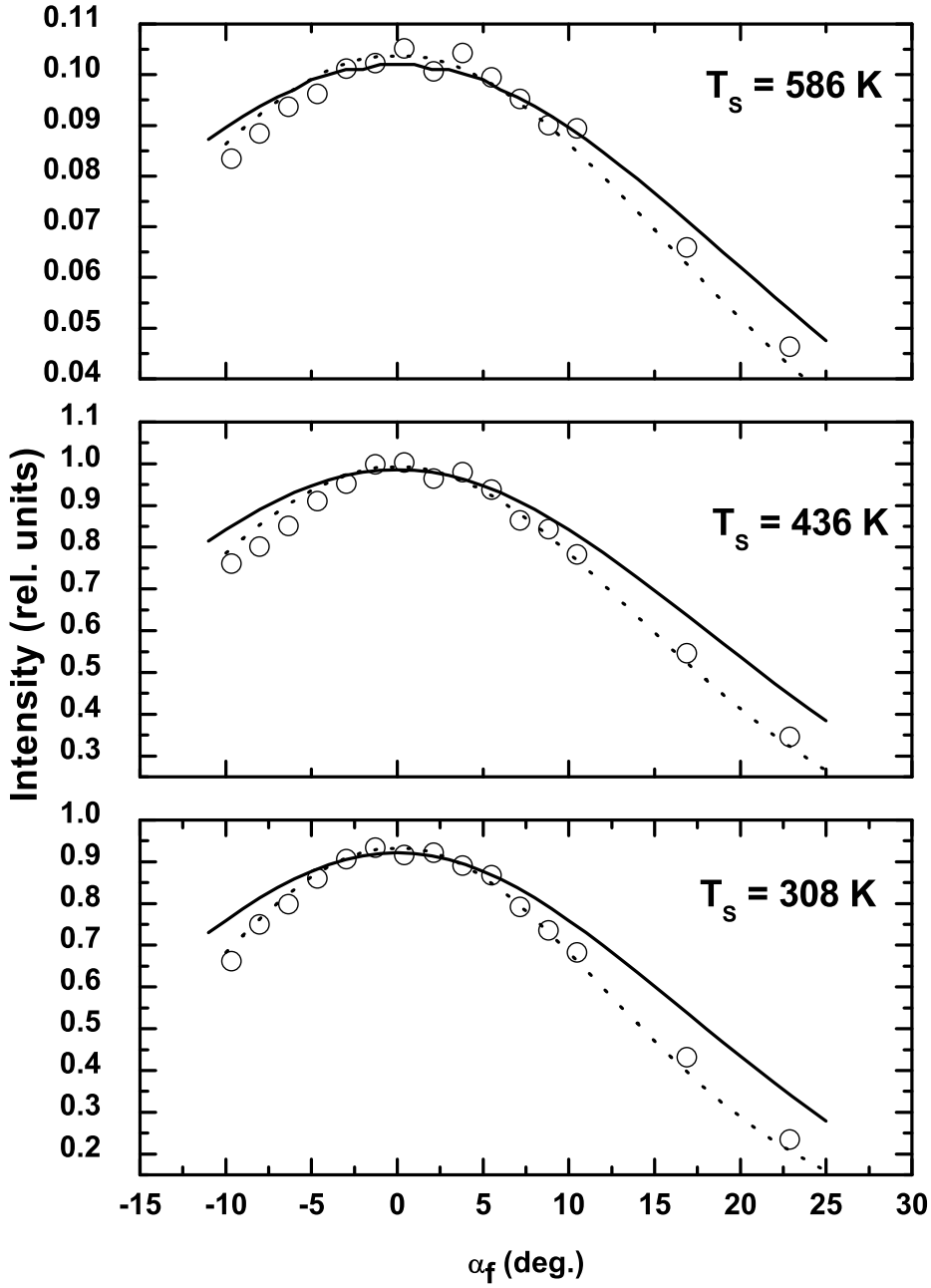

FIG. 4: Out-of-plane angular distributions for Ar scattering from molten Ga at $T_S = 308,\ 436,$ and 586 K as marked. The incident energy is $E_i = 92$ kJ/mol and the incident and final polar angles are $\theta_i = \theta_f = 55°$. The angle α_f is measured in the direction perpendicular to the scattering plane as explained in the text. Open circles are the data[15], the solid curve is the present calculation for a corrugated surface, and the dotted curve is for an uncorrugated surface.

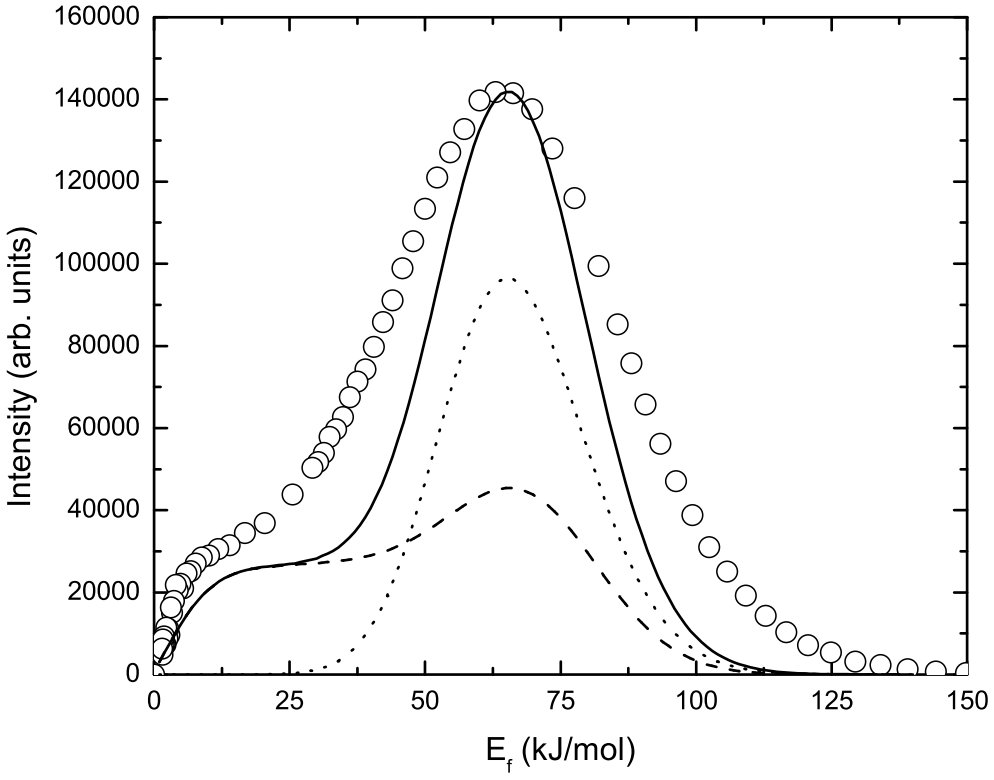

FIG. 5: Energy-resolved spectra of Ar scattering from molten Ga at $E_i = 95$ meV, $T_S = 483$ K, and $\theta_i = \theta_f = 55°$ including double scattering contribution.

only the shape of the broad single-peaked curves to model calculations does not provide an easy way to distinguish features of the interaction potential.

To complete the description of the scattering of 1 eV Ar from molten Ga we discuss here the origins of the prominent shoulder feature that appears in all the experimental energy-resolved spectra of Fig. 1. Figure 5 shows the same experimental data as in the middle panel of Fig. 1 for a molten Ga temperature of 483 K. Three calclulated curves appear in this figure. The dotted curve is the result of the corrugated model, the same as in Fig. 1. The dashed curve is the contribution from double collisions arising from a ring of six Ga atoms in the surface plane surrounding the original Ga atom at the average interparticle spacing, but with an average over azimuthal orientation angles of the six-atom ring in the surface plane.[38] Both the single scattering and the single plus double scattering, shown as

the solid curve, explain the shape of the large peak nearly equally well, but the double scattering contribution shows that the shoulder feature at very low energy comes primarily from double collisions. The trajectories that contribute to the shoulder are ones in which the Ar initially scatters backwards from a first collision with a Ga atom and then is scattered again in the forward direction in the scattering plane by a second Ga atom located on the surface in the region behind the first one. Both of these two collisions have a large scattering angle, each of which results in large energy loss, and the sum of these energy losses is what causes the relatively large-intensity shoulder at very low energies. However, it is interesting to note that the temperature dependence of the most probable intensity, as shown in Fig. 2, is not strongly affected by the double scattering contribution and the same value for the corrugation amplitude h is obtained using either the single or single plus double scattering calculation.

For the same Ar and molten Ga system additional temperature dependent data has been published for an incident Ar energy of 42 kJ/mol (435 meV). Figure 6 shows the most probable intensity as a function of temperature ranging from just above 300 to more than 460 K, the incident and final angles are both 55° and the designations of the calculated curves are the same as in Fig. 2. At this incident energy the corrugated surface calculation, shown as the solid curve, explains the data quite well with a corrugation parameter $h = 0.07$. When combined with the interparticle spacing of 2.78 Å for liquid Ga this value of h implies a height amplitude of 0.2 Å for the top of a Ga atom above the average surface level as sensed by the incoming Ar. This is considerably smaller than the corresponding value of 0.36 Å obtained from Fig. 2 for 95 kJ/mol Ar. It is expected that the corrugation of a soft amorphous metal surface would increase with the energy of the projectile due to larger penetration of the projectile into the relatively soft electron cloud of the amorphous surface.

The remaining system for which temperature dependence can be used to extract the corrugation amplitude is Ar scattering from molten In. Although this system has been discussed in an earlier letter,[19] we include it here for completeness. Figure 7 shows scattering spectra for 42 kJ/mol Ar scattering from liquid In at a temperature of 436 K and an incident angle $\theta_i = 55°$. Panel (a) shows an energy resolved spectrum for a detector angle at the specular position of $\theta_f = 55°$ with calculations similar to those of Fig. 5. Panels (b) shows the in-plane angular distribution, and panel (c) is the out-of-plane angular distribution taken also with the final angle $\theta_f = 55°$. Again, as for the case of Ar/Ga, the corrugated

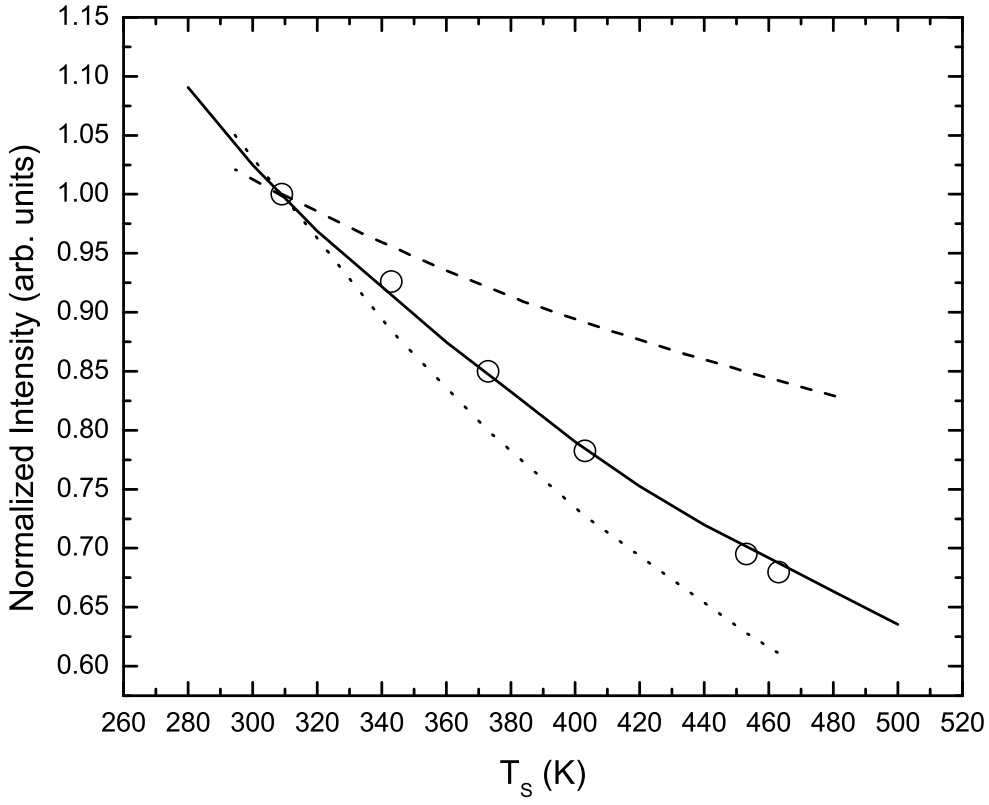

FIG. 6: Temperature dependence of the most probable intensity for a 42 kJ/mol incident beam of Ar scattering from molten Ga with $\theta_i = \theta_f = 55°$. The data points are from Nathanson *et al.*[14] and the calculations are designated similarly to those of Fig. 2.

and uncorrugated surface calculations are quite similar and both appear to explain the measured data[14,15] quite well. For these calculations the effective surface mass was taken to be the same as the mass of a single In atom and the parameter v_R is set to 450 m/s, the same as the values previously obtained from an analysis of this data using the uncorrugated model of Eq. (1).[38]

The temperature dependence of the most probable intensity of the measured energy resolved spectra is shown in Fig. 8 and, as was the case for molten Ga, it is this measurement that provides a significant difference in the results of calculations for a corrugated or uncorrugated surface and gives a more reliable means of determining the corrugation of

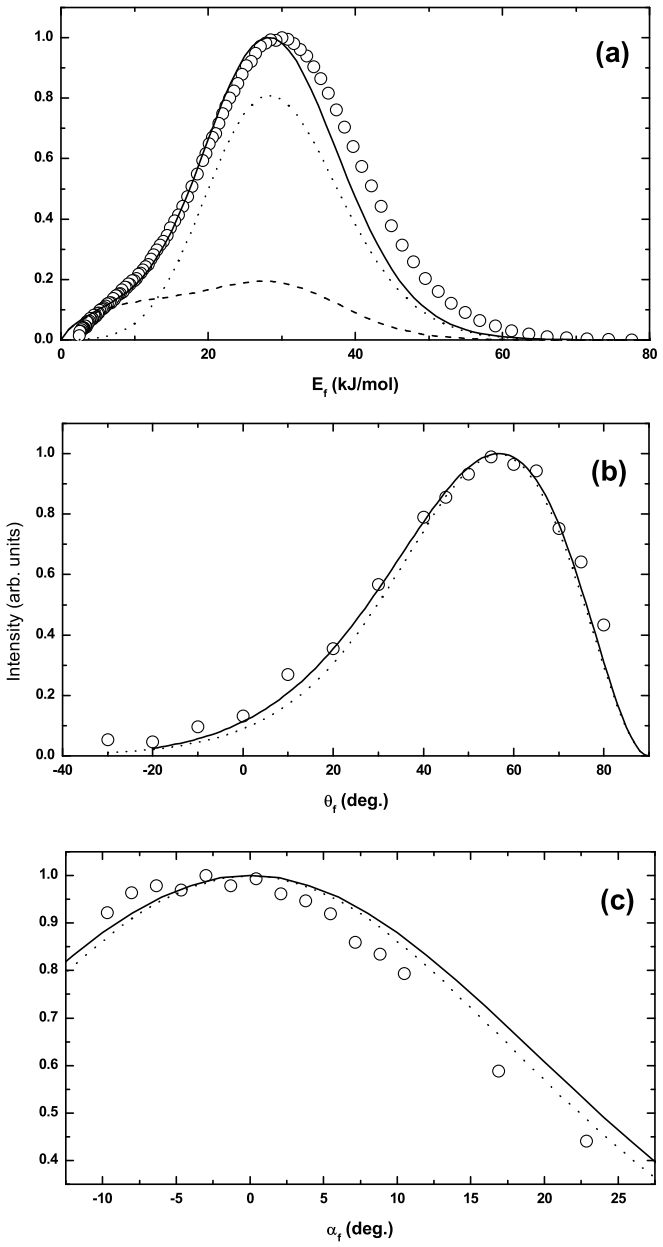

FIG. 7: Ar scattering from molten In at $T_S = 436$ K with an incident energy of 42 kJ/mol: (a) energy resolved spectrum for $\theta_i = \theta_f = 55°$, (b)in-plane angular distribution and (c) out-of-plane angular distribution both with $\theta_i = 55°$. The data points are from Nathanson et al.[14,15]

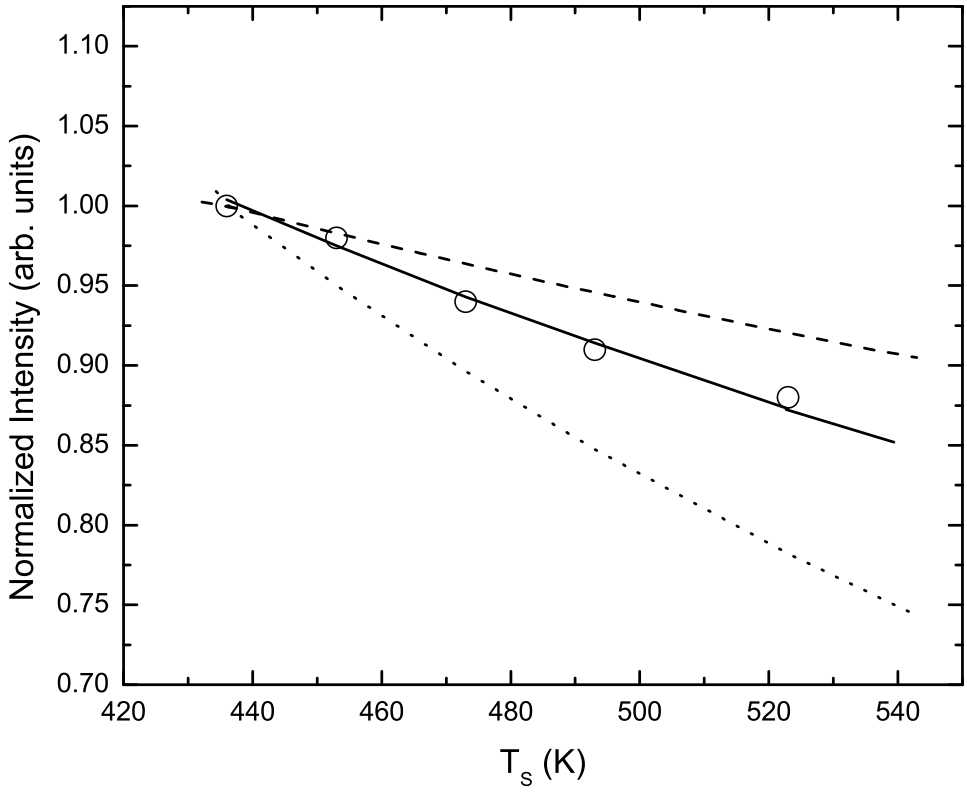

FIG. 8: Temperature dependence of the most probable intensity for Ar with energy 42 kJ/mol scattering from molten In with $\theta_i = \theta_f = 55°$. The data points are from Nathanson et al.[14] and the calculations are designated similarly to those of Figs. 2 and 6.

the potential. The solid curve match to the data was calculated using the corrugation of Eq. (14) with the corrugation amplitude $h = 0.29$. For the In liquid interatomic distance of $a = 3.14$ Å this gives a corrugation amplitude for a typical atom at the liquid surface of $ha = 0.91$ Å.

IV. DISCUSSION AND CONCLUSIONS

In this paper we have developed a theory, based on semiclassical quantum mechanics in the eikonal approximation, that can treat energy transfer with the surface via phonon excitation. For elastic scattering, including diffraction, it reduces to the eikonal theory of

Spadacini *et al.*[16], but with the additional feature that it includes a Debye-Waller factor. For single-quantum excitation processes it produces straightforward expression for describing the intensity spectra for single phonon creation or annihilation as developed in the appendix. The theory can be extended to the classical limit of multiphonon transfer, essentially giving an interesting and useful example of the Bohr correspondence principle of large quantum numbers. This limit is an extension of the classical atom-surface scattering theory of Brako and Newns[23] to the case of corrugated surfaces, in which the corrugation may be either ordered as for crystalline surfaces or disordered and amorphous as is the case for liquids.

The theory presented here, due to the fact that it is developed within the framework of the semiclassical eikonal approximation, is strictly valid only in the weak corrugation limit. As the corrugation is made weaker it goes to the flat surface case first considered by Brako and Newns as presented in Eq. (2). However the development also illustrates how the extreme large corrugation amplitude case of a surface of isolated scattering centers, as shown in Eq. (1) can be obtained when the corrugation is initially taken to be very strong. Thus this theory is intended to be a useful model for predicting the response to experimentally controllable parameters of gas-surface interaction systems in the classical regime, examples of experimentally controllable parameters being the temperature, incident energy, incident or final scattering angles, the effective mass of the surface, and even projectile atomic species.

The primary interest of the present theoretical developments is the result for scattering from corrugated surfaces in the classical mechanical regime, although interesting quantum mechanical results are presented in the Appendix A. This appendix includes useful results for elastic diffraction and for single phonon inelastic scattering, as well as an indication of how the double-phonon and higher orders of coherent quantum scattering can be developed. These quantum expressions illustrate that quantum spectra from ordered surfaces contain relatively sharp peaks for elastic scattering, particularly for diffraction, and for single quantum excitation of surface-specific phonons such as the Rayleigh mode.

In contrast to the quantum case the classical limit is distinguished by the Debye-Waller factor becoming vanishingly small, for example at high incident energies, large projectile masses, or large temperatures. In the classical limit all uniquely quantum features such as diffraction peaks or single phonon peaks disappear, and what is left behind is a much broader multi-quantum background. It should be noted that the classical limit is actually the limit of quantum decoherence due to large quantum numbers of phonon excitations.

Thus this quantum decoherence can occur even under some special circumstances in which the scattering conditions are still quantum mechanical, in the sense that the de Broglie wavelength of the projectile can be large. An example of such a possible situation would be scattering of low mass atoms at very low incident energies, but with the surface at high temperature which would lead to high probability of multiphonon excitations.

It is clear that scattering spectra observed under classical multiphonon conditions will be capable of providing much less information about the interaction potentials as compared with measurements done under quantum mechanical conditions. Compared to quantum mechanical spectra, which can contain sharp diffraction and single-phonon inelastic peaks, the rather broad and relatively featureless peaks observed in the classical regime will provide less detailed information on the interaction process. Nevertheless, scattering experiments under classical conditions can still provide important information about the interaction potential and the dynamics of the collision process. Examples are the determination of collective effects as evidenced by effective masses of the surface being different from that of single surface atoms, evidence for multiple collisions such as the double backscattering peak evident in Figs. 5 and 7, obtaining corrugation shapes from rainbow features, or determining the corrugation amplitude as emphasized here.

Although information about the corrugation of the surface could be obtained by comparing this theory to experiments, and particularly those done under conditions that exhibit classical rainbow behavior, we have shown here that the corrugation amplitude is readily extracted upon examination of the temperature dependence of the most probable amplitudes of energy-resolved atom-surface scattering spectra. By examining data for the scattering of supersonic beams of Ar from molten metal surfaces we determine that the corrugation amplitude of the interaction potential for liquid Ga is approximately 10% of the interatomic spacing, and for liquid In the amplitude is about 30% of the interatomic distance.

Although we have demonstrated that the temperature dependence of energy-resolved scattering spectra measured in the classical regime is sensitive to the corrugation amplitude, the same cannot be said about the shape of the spectra. Comparisons between the present theory with corrugation and previous calculations for a flat surface, such as exhibited in Figs. 3 and 7, show that the relative shape of the energy-resolved spectra calculated with or without corrugation are quite similar. For otherwise fixed experimental parameters such as energy and initial and final angles the corrugation makes a much greater effect on the

temperature dependence. The similarity of the corrugated and uncorrugated calculations illustrates a difficulty of trying to obtain a complete picture of the interaction potential using measurements carried out in the classical regime, especially when limited to a small range of incident energies and scattering angles. This is also a good illustration of the fact that there is typically much less information that can be obtained from experiments done in the classical domain, relative to those done in the quantum mechanical regime. It appears that in order to obtain useful and detailed information on the interaction potentials from measurements executed only in the classical domain it will be necessary to carry out experiments over very large ranges of incident and final angles as well as large ranges of incident energies.

An important question in the field of molecule-surface scattering can be addressed based on the results of calculations presented here and this is the question of the relative importance of the two mechanisms, corrugation or inelastic transfers to phonons, in forming the widths of measured angular distributions in scattering experiments using monoenergetic and angularly well-defined incident beams. Two differing theoretical approaches seem to indicate that either corrugation or phonons can cause the rather large angular widths over which well-defined incident molecular beams can scatter from surfaces under classical conditions. The washboard model of Tully[39] is extensively used to interpret experimental data and often gives good comparisons with experiments for the angular spread of the angular distributions in spite of the fact that it does not include a mechanism for energy transfer with the surface. However, theories that include energy transfer involving large numbers of excited phonons, such as those based on the Brako-Newns approach embodied in Eq. (2) also explain many experimental measurements rather well.[38,40] The work presented here indicates that both static corrugations as well as energy and momentum transfer through phonons can contribute equally to similar angular spreads in measured angular distributions. As mentioned above, this work appears to indicate that in order to separate and define the importance of the two contributions of corrugation and phonons it will require extensive comparisons of experimental measurements over large ranges of angles and energies.

APPENDIX A: QUANTUM MECHANICAL LIMITS

Although the main results of this paper, and all comparisons with experiments, are for scattering in the classical limit the central expression from which the classical results are derived, i.e., Eq. (10), is fully quantum mechanical within the semiclassical approximation. It is of interest to present the quantum results obtained from Eq. (10) for elastic and single-phonon inelastic transfer. The classical results were obtained by evaluating the correlation function $2\mathcal{W}(\mathbf{p};\mathbf{R},\mathbf{R}',t)$ of Eq. (9) in the classical limit where its important contributions come from small times and spatial separations, as shown in Eq. (12). In the quantum limit the contributions from the correlation function extend to larger times and separations, and a development in terms of ordered numbers of phonons transferred in the collision is obtained by expanding the exponential in the transition rate of Eq. (10) as

$$\exp\{2\mathcal{W}(\mathbf{p};\mathbf{R},\mathbf{R}',t)\} \;=\; 1 \;+\; 2\mathcal{W}(\mathbf{p};\mathbf{R},\mathbf{R}',t) \;+\; 2\;\mathcal{W}^2(\mathbf{p};\mathbf{R},\mathbf{R}',t) \;+\; \ldots \quad . \tag{A1}$$

The constant term in the expansion leads to elastic scattering, the first order term gives contributions due to single phonon excitation, the second order term gives double phonon transfers, etc.

1. Elastic scattering

The elastic scattering contribution comes from retaining only the leading term in Eq. (A1) in which case the transition rate of Eq. (10) becomes

$$w(\mathbf{p}_f,\mathbf{k}_i) \;=\; \frac{2\pi}{\hbar}\,|T_{fi}|^2 \;\; e^{-2W(\Delta\mathbf{k})}\;\delta(E_f-E_i)\;. \tag{A2}$$

where the transition matrix T_{fi} is identical with that of the elastic eikonal approximation of Eq. (6). For scattering from an arbitrary surface, this is consistent with the result obtained in Ref. [16] except that it now contains the addition of the Debye-Waller factor which gives the attenuation of the elastic signal due to inelastic scattering.

In the case in which the scattering is from an ordered, periodic surface the only scattering is into the diffraction peaks appearing at the positions denoted by the conditions of conservation of energy $E_f = E_i$ and parallel momentum transfer given by a wave vector equal to

a surface reciprocal vector $\mathbf{G}$ according to $\mathbf{K} = (\mathbf{P}_f - \mathbf{P}_i)/\hbar = \mathbf{G}$.

$$w^{(0)}(\mathbf{k}_f, \mathbf{k}_i) \;=\; \frac{2\pi}{\hbar} \sum_{\mathbf{G}} |T_{\mathbf{G},i}|^2 \; e^{-2W(\Delta\mathbf{k})} \; \delta(\mathbf{K}_f - \mathbf{K}_i - \mathbf{G}) \; \delta(E_f - E_i) \; . \tag{A3}$$

The transition matrix of Eq. (6) is evaluated over a single unit cell ($u.c.$) of surface area $S_{u.c.}$ and is given by

$$T_{\mathbf{G},i} \;=\; -\frac{\hbar p_{fz}}{mL} \frac{1}{S_{u.c.}} \int_{u.c.} d\mathbf{R} \; e^{-i\mathbf{G}\cdot\mathbf{R}} \; e^{-i\Delta k_{\mathbf{G},z}\xi(\mathbf{R})} \quad , \tag{A4}$$

where the value of the perpendicular wave vector transfer $\Delta k_{\mathbf{G},z}$ is fixed for each diffraction peak $\mathbf{G}$ by the conservation of energy and parallel momentum.[16]

2. Single phonon inelastic scattering

The transition rate for single quantum excitation is obtained from Eq. (10) by retaining only the first order term in the expansion of the correlation function of Eq. (A1). This leads to

$$\begin{aligned} w(\mathbf{p}_f, \mathbf{k}_i) \;=\; & \frac{1}{\hbar^2} \left(\frac{\hbar^2 k_{fz}}{mL}\right)^2 \int_{-\infty}^{+\infty} dt \; e^{i(E_i - E_f)t/\hbar} \; \frac{1}{L^4} \int d\mathbf{R} \int d\mathbf{R}' \\ \times \; & e^{-i\mathbf{K}\cdot(\mathbf{R}-\mathbf{R}')} \; e^{-i\Delta k_z[\xi(\mathbf{R})-\xi(\mathbf{R}')]} \; e^{-2W(\Delta\mathbf{k})} \; \langle \; \mathbf{k}\cdot\mathbf{u}(\mathbf{R},t) \; \mathbf{k}\cdot\mathbf{u}(\mathbf{R}',0) \; \rangle \; . \end{aligned} \tag{A5}$$

The above is as far as one can go without additional knowledge about the nature of the vibrations of the surface. An interesting case, and the one most often used, is that of a periodic crystalline surface. Assuming a Bravais lattice with only a single atom per unit cell denoted by its lattice site number l the displacement correlation function becomes very similar to the form used in neutron or X-ray scattering:[41]

$$\begin{aligned} \langle \mathbf{k}\cdot\mathbf{u}_{l'} \; \mathbf{k}\cdot\mathbf{u}_l \rangle \;=\; & \sum_{\alpha,\alpha'=1}^{3} k_\alpha k_{\alpha'} \sum_{\mathbf{Q},\nu} \frac{\hbar}{2NM_S\omega_\nu(\mathbf{Q})} \; e_\alpha(\mathbf{Q},\nu) \; e^*_{\alpha'}(\mathbf{Q},\nu) \; e^{i\mathbf{Q}\cdot(\mathbf{R}_l - \mathbf{R}_{l'})} \\ & \times \; \{[2n(\omega_\nu(\mathbf{Q})) + 1]\cos(\omega_\nu(\mathbf{Q})) \; - \; i\sin(\omega_\nu(\mathbf{Q}))\} \quad , \end{aligned} \tag{A6}$$

where $\omega_\nu(\mathbf{Q})$ is the frequency of a surface phonon of parallel wave vector $\mathbf{Q}$ and other quantum numbers ν, the Bose-Einstein function is

$$n(\omega_\nu(\mathbf{Q})) \;=\; \frac{1}{e^{\frac{\hbar\omega_\nu(\mathbf{Q})}{k_B T_S}} \; - \; 1} \quad , \tag{A7}$$

and $e_\alpha(\mathbf{Q},\nu)$ is the phonon polarization vector in the cartesian direction denoted by α. Parallel wave vectors are treated in the extended zone scheme.

The transition rate for single phonon transfer is conveniently written in terms of the surface phonon spectral density, essentially the Fourier transform of the displacement correlation function evaluated at zero temperature, which is defined by

$$\rho_{\alpha,\alpha'}(\mathbf{K},\omega) \;=\; \sum_\nu \frac{\hbar}{2\; S_{u.c.}\; M_S\; \omega_\nu(\mathbf{K})}\; e_\alpha(\mathbf{K},\nu)\; e^*_{\alpha'}(\mathbf{K},\nu)\; \delta(\omega-\omega_\nu(\mathbf{K})) \quad . \tag{A8}$$

In terms of the phonon spectral density the transition rate for single phonon transfer becomes

$$\begin{aligned} w^{(1)}(\mathbf{k}_f,\mathbf{k}_i) \;&=\; \frac{2\pi S_{u.c.}}{\hbar} \sum_{\alpha,\alpha'=1}^{3} k_\alpha k_{\alpha'}\; |T_{fi}|^2\; e^{-2W(\mathbf{k})} \\ \times\;& \{\rho_{\alpha,\alpha'}(-\mathbf{K},-\omega)\; [n(\omega)+1] \;+\; \rho_{\alpha,\alpha'}(\mathbf{K},\omega)\; n(\omega)\} \quad . \end{aligned} \tag{A9}$$

The term in proportional to $[n(\omega)+1]$ describes phonon creation and the term in $n(\omega)$ is for phonon annihilation.

Within the eikonal approximation that we have used in this paper, the transition matrix has a form that appears similar to Eq. (6), but with the final momenta taking on a new meaning:

$$T_{fi} \;=\; -\frac{\hbar^2 k_{fz}}{mL}\; \frac{1}{S_{u.c.}} \int_{u.c.} d\mathbf{R}\; e^{-i\mathbf{K}\cdot\mathbf{R}}\; e^{-i\Delta k_z \xi(\mathbf{R})} \quad , \tag{A10}$$

where $\mathbf{k} = \{\mathbf{K}, k_z\} = (\mathbf{p}_f - \mathbf{p}_i)/\hbar$ with the final momentum $\mathbf{p}_f$ defined by including the energy and momentum transferred to the phonon that is created or annihilated, i.e., via the energy conservation law which is $E_f - E_i = \hbar\omega$ and the momentum conservation law which applies only to the parallel direction and is given by $\mathbf{P}_f - \mathbf{P}_i = \hbar\mathbf{K}$. Thus, in the eikonal approximation the transition matrix for inelastic scattering is the matrix element of the elastic potential operator, but extended off the elastic energy shell, i.e., the matrix element is taken with respect to eignestates corresponding to the initial and final momenta of the inelastic scattering states.

* Electronic address: Wayne.Hayes@gvltec.edu

† Electronic address: jmanson@clemson.edu

[1] G. Benedek and J. P. Toennies, Surf. Sci. **299**, 587 (1994).

[2] G. Benedek, M Bernasconi, V. Chis, E. Chulkov, P. M. Echenique, B. Hellsing and J. P. Toennies, J. Phys. Condens. Matter **22** 084020 (2010).

[3] E. Hulpke, editor, *Springer Series in Surface Sciences*, Vol. 27, Springer-Verlag, Heidelberg (1992).

[4] D. Farías and K.-H.Rieder, Reports on Progress in Physics **61** 1575 (1998).

[5] A. P. Jardine, S. Dworski, P. Fouquet, G. Alexandrowicz, D. J. Riley, G. Y. H. Lee, J. Ellis, and W. Allison, Science **304**, 1790 (2004).

[6] J. A. Barker and D. J. Auerbach, Faraday Discussions **80**, 277 (1985).

[7] A. W. Kleyn and T. C. M. Horn, Physics Reports **199**, 192 (1991).

[8] B. Gumhalter, Phys. Rep. **351**, 1 (2001).

[9] Eli Pollak and Salvador Miret-Artés, J. Chem. Phys. **130**, 194710 (2009).

[10] E. Pollak, Jeremy M. Moix and Salvador Miret-Artés, Phys. Rev. B **80**, 165420 (2009).

[11] E. Pollak, S. Sengupta and S. Miret-Artés, J. Chem. Phys. **129**, 054107 (2008).

[12] Jeremy M. Moix, Eli Pollak and Salvador Miret-Artés, Phys. Rev. Lett. **104**, 116103 (2010).

[13] *Handbook of Surface Science*, edited by N. V. Richardson and S. Holloway, Vol. 3 "Surface Dynamics", edited by E. Hasselbrink and B. Lundqvist (Elsevier, Amsterdam, 2008).

[14] W. R. Ronk, D. V. Kowalski, M. Manning, and G. Nathanson, J. Chem. Phys. **104**, 4842 (1996).

[15] Michelle Manning, Jason A. Morgan, David J. Castro and Gilbert M. Nathanson, J. Chem. Phys. **119**, 12593 (2003).

[16] U. Garibaldi, A. C. Levi, R. Spadacini and G. Tommei, Surface Science **48**, 649 (1975).

[17] V. Bortolani and A. C. Levi, Riv. del Nuovo Cimento **9**, 1 (1986).

[18] J. R. Manson, Phys. Rev. B **58** , 2253 (1998).

[19] W. W. Hayes and J. R. Manson, Phys. Rev. Lett. **109**, 063203 (2012).

[20] A. Sjölander, Ark. Phys. **14**, 315 (1959).

[21] D. A. Micha, J. Chem. Phys. **74**, 2054 (1981).

[22] J. R. Manson, Phys. Rev. B **43**, 6924 (1991).

[23] R. Brako and D. M. Newns, Phys. Rev. Lett. **48**, 1859 (1982); R. Brako and D. M. Newns, Surf. Sci. **117**, 422 (1982).

[24] H.-D. Meyer and R. D. Levine, Chem. Phys. **85**, 189 (1984).

[25] J. R. Manson, V. Celli and D. Himes, Phys. Rev. B **49**, 2782 (1994).

[26] J. Powers, J. R. Manson, C. E. Sosolik, J. R. Hampton, A. C. Lavery, and B. H. Cooper, Phys. Rev. B **70** 115413 (2004).

[27] Massimo F. Bertino, J. R. Manson, and W. Silvestri, J. Chem. Phys. **108**, 10239 (1998).

[28] G. Armand, J. R. Manson and C. S. Jayanthi, Phys. Rev. B **34**, 6627 (1986).

[29] W. W. Hayes and J. R. Manson, J. Phys.: Condens. Matter **23**, 484003 (2011).

[30] E. Pollak and J. R. Manson, J. Phys. Condens. Matt. **24**, 104001 (2012).

[31] R. Glauber, Phys. Rev. **87**, 189 (1952).

[32] L. Van Hove, Phys. Rev. **95**, 249 (1954).

[33] O. Stern, Naturwissenschaften **17**, 391 (1929).

[34] I. Estermann and O. Stern, Z. Phys. **61**, 95 (1930).

[35] G. Brusdeylins, H.-D. Meyer, J. P. Toennies, and K. Winkelmann, in *Rarefied Gas Dynamics* Vo. 51, Part II, ed. by J. L. Potter, AIAA, New York, p. 1047 (1977).

[36] R. Campargue, A. Lebehot, and J. C. Lemmonnier, in *Rarefied Gas Dynamics* Vo. 51, Part II, ed. by J. L. Potter, AIAA, New York, p. 1033 (1977).

[37] J. E. Hurst, C. A. Becker, J. P. Cowin, K. C. Janda, L. Wharton and D. J. Auerbach, Phys. Rev. Lett. **43**, 1175 (1979).

[38] W. W. Hayes and J. R. Manson, J. Chem. Phys. **127**, 164714 (2007).

[39] J. C. Tully, J. Chem. Phys. **92**, 680, (1990).

[40] V. Celli, D. Himes, P. Tran, J. P. Toennies, C. Wöll, G. Zhang, Phys. Rev. Lett. **66**, 3160 (1991).

[41] A. A. Maradudin, E. W. Montroll and G. H. Weiss, in *Solid State Physics: Theory of Lattice Dynamics in the Harmonic Approximation* (Academic Press, New York, 1963), Suppl. 3.

LIST OF FIGURES